

# Robust Floquet Topological Phases and Anomalous $\pi$ -Modes in Quasiperiodic Quantum Walks

F. Iwase\*

Department of Physics, Tokyo Medical University  
6-1-1 Shinjuku, Shinjuku-ku, Tokyo 160-8402, Japan

We uncover the global topological phase diagram of one-dimensional discrete-time quantum walks driven by Fibonacci-modulated coin parameters. Utilizing the mean chiral displacement (MCD) as dynamical probe, we identify robust topological phases defined by a strictly quantized winding number  $\nu = -1$  and exponentially localized edge states. Crucially, we discover that these topological edge modes emerge not only at zero energy but also at the quasienergy zone boundary  $E = \pi$ , exhibiting identical localization robustness despite the fractal nature of the bulk spectrum. These results demonstrate that Floquet topological protection remains intact amidst quasiperiodic disorder, offering a concrete route to observing exotic non-equilibrium phases in photonic experiments.

The discovery of topological phases of matter has triggered a paradigm shift in modern condensed matter physics, shifting the focus from local order parameters to global invariants [1–3]. While this framework is well-established for periodic crystals relying on Bloch’s theorem, a critical frontier lies in quasicrystals—structures that lack translational symmetry yet possess long-range order [4, 5]. In these landscapes of “ordered disorder,” a fundamental question arises: how does the robust bulk-edge correspondence compete with the tendency toward Anderson localization? Elucidating this interplay is crucial, as the breakdown of periodicity may lead not merely to the destruction of topological phases, but to the emergence of novel phase diagrams and critical states unique to fractal environments [6, 7].

Discrete-time quantum walks (DTQWs) serve as a versatile platform to address this challenge [8]. As inherently periodically driven Floquet system, DTQWs offer exceptional controllability over evolution operators, enabling the precise engineering of topological phases hosted by chiral symmetry [9]. Although quantum dynamics in Fibonacci-modulated systems have been explored previously, attention has largely been confined to anomalous diffusion kinetics or the multifractal geometry of energy spectra [10–12]. Consequently, a comprehensive understanding of the global topological phase diagram and the underlying mechanism of phase transitions driven by quasiperiodicity remains largely unexplored.

In this Letter, we present a comprehensive study of topological phases in one-dimensional quantum walks driven by Fibonacci-modulated coin parameters. To rigorously address the quasiperiodicity, we employ a systematic sequence of rational approximants based on Fibonacci numbers, allowing us to control finite-size effects precisely. Furthermore, by performing long-time averaging of the mean chiral displacement (MCD), we effectively eliminate transient fluctuations and successfully extract quantized topological invariants directly from the bulk dynamics, even in the presence of aperiodic modulation.

Our study reveals three key findings. First, we uncover a global phase diagram featuring a fractal structure in the parameter space. The phase boundaries exhibit a striking resemblance to the Hofstadter butterfly, reinforcing the topological equivalence between 1D quasiperiodic systems and 2D integer quantum Hall systems [13]. Second, we demonstrate the coexistence of topological edge states at both zero and  $\pi$  quasienergies. This highlights the unique Floquet nature of the system, distinguishing it from static quasiperiodic models. Third, by analyzing the localization length, we demonstrate the existence of robust edge states at both zero and  $\pi$  quasienergies. Remarkably, these modes exhibit an identical average lo-

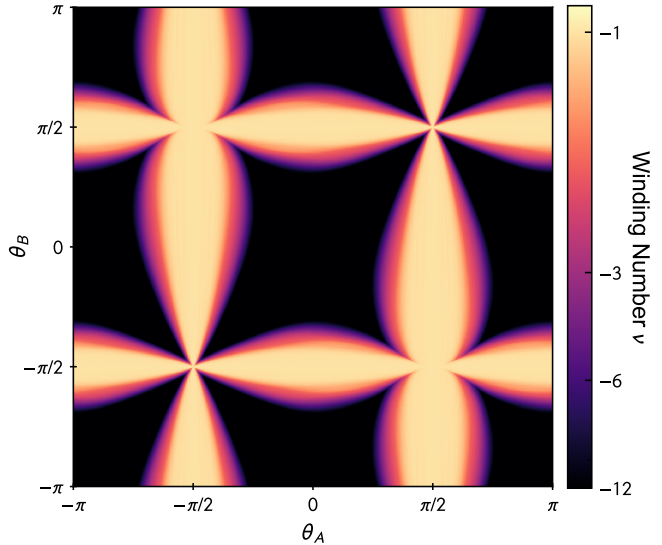


FIG. 1. (Color online) Global topological phase diagram. The winding number  $\nu$ , extracted from the mean chiral displacement (MCD), is mapped in the  $(\theta_A, \theta_B)$  parameter plane for  $N = F_{18} = 2584$ . Yellow regions indicate the topological phase ( $\nu \approx -1$ ), while dark regions correspond to metallic or gapless regimes. The color scale is saturated at  $-12$  for visibility; actual MCD values in the metallic regions reach  $\sim -1200$ .

calization length, despite their distinct microscopic oscillation patterns arising from the quasiperiodic potential. This indicates that the inherent chiral symmetry protects Floquet topological phases even in the presence of strong aperiodic disorder.

We consider a DTQW on a one-dimensional lattice with  $N$  sites [14]. The Hilbert space is defined as  $\mathcal{H} = \mathcal{H}_P \otimes \mathcal{H}_C$ , spanned by the position states  $\{|x\rangle\}_{x \in \mathbb{Z}}$  and the coin states  $\{|L\rangle, |R\rangle\}$ , representing the internal degrees of freedom. The time evolution of the system is governed by the unitary operators  $U = S \cdot U_C$ , where one step of the walk is given by  $|\psi(t+1)\rangle = U|\psi(t)\rangle$ . The shift operator  $S$  moves the walker to the left or right depending on the coin state:

$$S = \sum_x (|x-1\rangle\langle x| \otimes |L\rangle\langle L| + |x+1\rangle\langle x| \otimes |R\rangle\langle R|). \quad (1)$$

The coin operator  $U_C$  performs a site-dependent rotation on the internal states:

$$U_C = \sum_x |x\rangle\langle x| \otimes M(\theta_x), \quad M(\theta_x) = \begin{pmatrix} \cos \theta_x & \sin \theta_x \\ -\sin \theta_x & \cos \theta_x \end{pmatrix}, \quad (2)$$

where  $\theta_x$  is the rotation angle at site  $x$ .

To introduce quasiperiodicity, we modulate the coin parameter  $\theta_x$  according to the Fibonacci sequence [6]. The sequence is generated recursively by the concatenation rule  $S_{j+1} = S_j S_{j-1}$  with  $S_0 = "B"$  and  $S_1 = "A"$ . In the limit of  $j \rightarrow \infty$ , the ratio of the number of "A" sites to "B" sites converges to the golden mean  $\tau = (1 + \sqrt{5})/2$ , realizing a quasiperiodic modulation. We assign two distinct parameter values,  $\theta_A$  and  $\theta_B$ , to the letters "A" and "B" in the sequence, respectively. For numerical simulations, we employ the periodic approximant method using the  $j$ -th Fibonacci number  $F_j$  (e.g.,  $N = F_{18} = 2584$ ) as the system size.

The present system possesses chiral symmetry and belongs to the AIII class [15]. The topological phase can be characterized by the winding number  $\nu \in \mathbb{Z}$  [9]. In 1D quantum walks, this invariant is directly accessible through the MCD [16, 17]. The MCD at time  $t$  is defined as the expectation value of the displacement operator weighted by the chiral operator  $\Gamma = \sigma_z$ :

$$C(t) = \langle \psi(t) | (\hat{x} - x_0) \otimes \sigma_z | \psi(t) \rangle, \quad (3)$$

where  $\hat{x}$  is the position operator and  $x_0$  is the initial position. To eliminate transient oscillations and ensure convergence to the true topological invariant, we evaluate the long-time average of the MCD:

$$\nu = 2 \times \lim_{T \rightarrow \infty} \frac{1}{T} \sum_t C(t). \quad (4)$$

For the calculation of the MCD, we employ periodic boundary conditions to simulate the bulk properties of

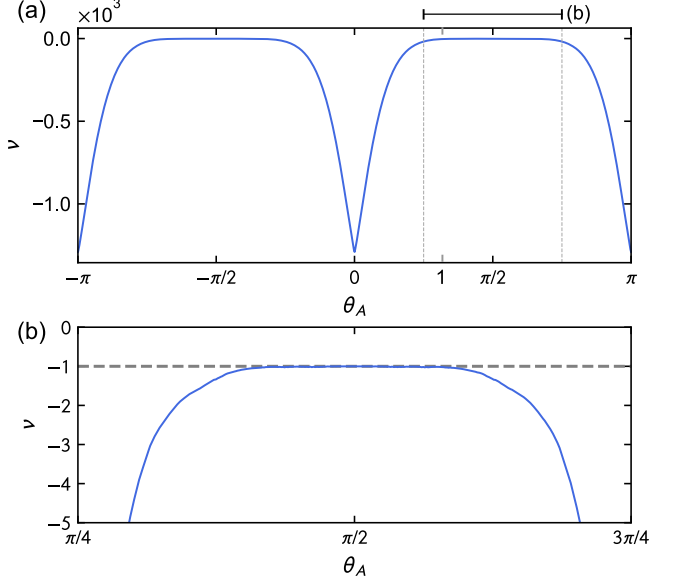


FIG. 2. (Color online) Topological phase transition and quantization. (a) The topological winding number  $\nu$ , defined as twice the long-time averaged mean chiral displacement (MCD), is plotted against  $\theta_A$  along the cut  $\theta_B = 0$ . Robust plateaus are observed in the topological regions (centered around  $\theta_A \approx \pm\pi/2$ ), whereas the metallic regions exhibit large fluctuations or asymptotic divergence, signifying the ballistic nature of the wave packet. (b) Magnified view of the topological regime ( $\pi/4 \leq \theta_A \leq 3\pi/4$ ), confirming a quantized plateau at  $\nu = -1$ .

the quasiperiodic lattice, with the time evolution truncated before the wave packet reaches the system boundaries. Conversely, to investigate the edge states and energy spectrum, we impose reflective boundary conditions to preserve the unitarity of the time-evolution operator.

Figure 1 illustrates the global topological phase diagram mapped in the  $(\theta_A, \theta_B)$  parameter space. The color scale represents the winding number  $\nu$ , evaluated via the MCD averaged over a duration sufficient to capture bulk dynamics (Eq. 4). The resulting landscape exhibits intricate, fractal-like boundaries that contrasts sharply with the simple phase boundaries typical of periodic systems [8]. Prominent bright yellow regions identify the topological phase characterized by a quantized winding number  $\nu = -1$ . In contrast, the dark regions correspond to gapless metallic phases where the topological invariant is ill-defined and the MCD exhibits large fluctuations associated with ballistic transport. This complex phase boundary reflects the underlying multi-fractal energy spectrum—reminiscent of the Hofstadter butterfly—which becomes explicitly visible in the periodic boundary condition spectrum as detailed in Fig. S1 (see the Supplemental Material [18] for the spectrum and a movie showing the time-evolution of the extended phase diagram).

To characterize the topological phase transition, we track the evolution of the winding number  $\nu$  along the cut line  $\theta_B = 0$ , as shown in Fig. 2. Approaching the metallic region (small  $|\theta_A|$ ), the MCD signals a breakdown of topological quantization, exhibiting large fluctuations and sharp increase in magnitude (Fig. 2(a)). This behavior signifies the onset of ballistic transport where the wave packet spreads extensively, corresponding to anomalous diffusion regime characteristic of the Fibonacci lattice [10].

In stark contrast, within the topological phase (e.g., around  $\theta_A \approx \pm\pi/2$ ), the MCD stabilizes precisely at the quantized integer value of  $\nu = -1$  (Fig. 2(b)). The robustness of this plateau against the quasiperiodic disorder is a hallmark of topological protection. This behavior is corroborates directly with the energy spectrum shown in Fig. S2 (Supplemental Material[18]); the emergence of the topological plateau coincides with the opening of a large macroscopic energy gap, whereas the metallic regions correspond to gapless bands exhibiting the ballistic spreading of the wave packet.

Finally, we provide direct evidence of the bulk-edge correspondence by examining the spatial structure of the topological edge states. Figure 3(a) displays the quasienergy spectrum calculated at  $\theta_A = 1$  and  $\theta_B = 0$ , where the bulk states exhibit a fragmented band structure characteristic of a Cantor set [6], reflecting the fractal nature of the Fibonacci potential. Crucially, isolated edge modes are clearly resolved within the energy gaps at both  $E \approx 0$  and  $E \approx \pi$ . To elucidate their properties, Fig. 3(b) depicts the spatial probability density  $|\psi(x)|^2$  of these modes, representing the behavior deep within the topological plateau. Both wavefunctions exhibit a pronounced peak at the system boundary, followed by a rapid exponential decay. Remarkably, the zero-energy and  $\pi$ -energy modes share an identical average decay rate, corresponding to an extremely tight localization length of  $\xi \approx 0.66$ . While the average slope is uniform, the decay tails are modulated by log-periodic oscillations, a signature reflecting the self-similar geometry of the underlying lattice. These results confirm that topological protection remains rigorous even in the absence of translational symmetry.

Our results underscore the unique interplay between topology and quasiperiodicity. A central finding of this work is the remarkable robustness of the topological edge states against the aperiodic modulation. In contrast to uncorrelated random disorder, where Anderson localization typically obliterates energy gaps and destroys topological phases [19], the quasiperiodic Fibonacci potential retains long-range structural correlations that preserve the global gap structure. Consequently, the topological edge modes remain rigorously protected, exhibiting the tight localization observed in Fig. 3, even amidst the intrinsic “ordered disorder” of the lattice.

Dynamically, this topological robustness is explicitly

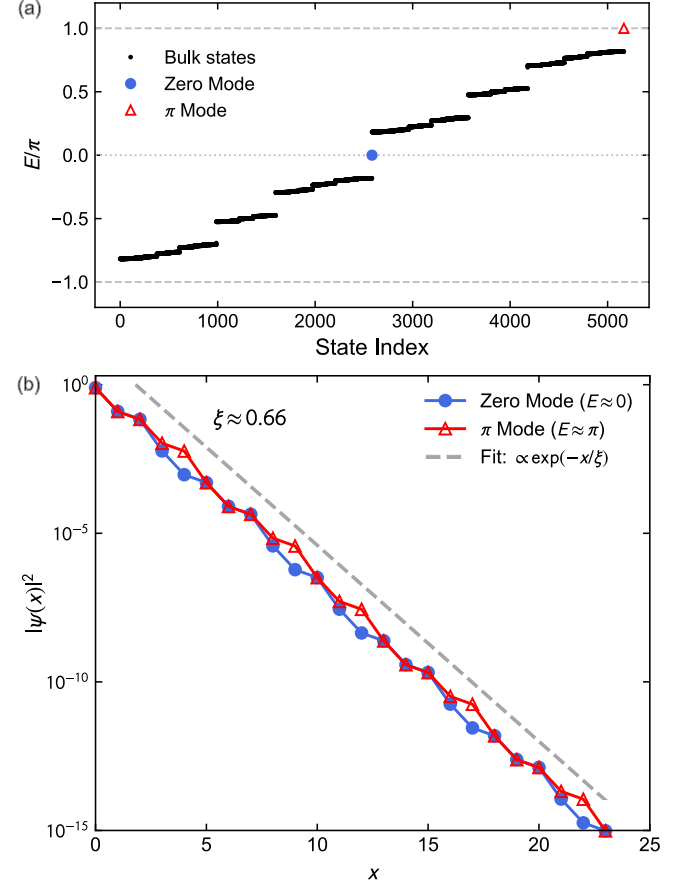


FIG. 3. (Color online) Topological edge states and their localization properties calculated at  $\theta_A = 1$  and  $\theta_B = 0$ . (a) Quasienergy spectrum. Bulk states are shown in black dots. The isolated zero-energy modes (solid royal blue circles) and  $\pi$ -energy modes (open red triangles) are clearly visible within the gaps. (b) Spatial probability distributions of the edge modes shown in (a). The zero mode (blue circles) and the  $\pi$  mode (red triangles) exhibit identical localization lengths, despite their distinct microscopic oscillation patterns. The  $\pi$  mode is spatially mirrored for comparison. The gray dashed line indicates the exponential fit with  $\xi \approx 0.66$ , shifted vertically for clarity.

manifested in the time-evolution of the MCD. Within the topological phase, the MCD converges strictly to the quantized integer  $\nu = -1$ , serving as a dynamical witness of the bulk winding number. In stark contrast, the metallic limit ( $\theta_{A,B} \rightarrow 0$ ) exhibits a breakdown of this quantization, characterized by an asymptotic divergence in the MCD magnitude. This divergence is not a failure of the indicator but a faithful dynamical signature reflecting the gapless nature of the spectrum where the topological invariant becomes ill-defined. Such a sharp dynamical distinction allows for the precise determination of phase boundaries based solely on bulk dynamics, offering a significant advantage for experimental detection.

Finally, the observation of edge states at the zone boundary ( $E = \pi$ ) corroborates the intrinsic Floquet nature of the topological phase, distinguishing it from static counterparts. Deep within the topological plateau, these  $\pi$ -modes exhibit a localization length ( $\xi \approx 0.66$ ) identical to that of the zero-energy modes, a symmetry enforced by the chiral constraint of the Hamiltonian. However, approaching the phase transitions, this tight confinement relaxes significantly; for instance, we observe a diverging tail ( $\xi \approx 40$ ) near the critical point  $\theta_A \approx 0$ . This contrast implies that the localization robustness is governed universally by the spectral gap magnitude—dictated by the distance from the critical points—regardless of whether the mode resides at zero or  $\pi$  energy, as evidenced by the global spectral evolution shown in the Supplemental Material. Collectively, these findings establish DTQWs as a prime candidate for exploring the critical interplay between the fractal disorder and Floquet topology.

In conclusion, we have elucidated the global topological phase diagram of DTQWs under Fibonacci quasiperiodic modulation. Our study reveals that robust topological phases, characterized by strictly quantized winding numbers and strong exponential localization, can coexist with a fractal energy landscape. These findings not only confirm the validity of the bulk-edge correspondence in the absence of translational symmetry but also extend the concept of topological protection to the non-equilibrium Floquet regime, hosting edge states at both zero and  $\pi$  energies. Crucially, our results highlight that chiral symmetry acts as a vital protector of topological order, ensuring that these phases persist even when translational symmetry is completely broken by quasiperiodicity. Given the high experimental feasibility of DTQWs using standard optical components—such as beam splitters and wave plates—our work provides a concrete blueprint for observing these exotic fractal topological phases. The demonstrated robustness of the edge states against quasiperiodic modulation paves the way for novel applications in topological photonics, including disorder-immune optical waveguides in aperiodic media.

---

\* iwasef@tokyo-med.ac.jp

- [1] M. Z. Hasan and C. L. Kane, Rev. Mod. Phys. **82**, 3045 (2010).
- [2] X.-L. Qi and S.-C. Zhang, Rev. Mod. Phys. **83**, 1057 (2011).
- [3] C.-K. Chiu, J. C. Y. Teo, A. P. Schnyder, and S. Ryu, Rev. Mod. Phys. **88**, 035005 (2016).
- [4] D. Levine and P. J. Steinhardt, Phys. Rev. Lett. **53**, 2477 (1984).
- [5] D. Shechtman, I. Blech, D. Gratias, and J. W. Cahn, Phys. Rev. Lett. **53**, 1951 (1984).
- [6] M. Kohmoto, L. P. Kadanoff, and C. Tang, Phys. Rev. Lett. **50**, 1870 (1983).
- [7] Y. E. Kraus, Y. Lahini, Z. Ringel, M. Verbin, and O. Zilberberg, Phys. Rev. Lett. **109**, 106402 (2012).
- [8] T. Kitagawa, M. S. Rudner, E. Berg, and E. Demler, Phys. Rev. A **82**, 033429 (2010).
- [9] J. K. Asbóth, Phys. Rev. B **86**, 195414 (2012).
- [10] S. Abe and H. Hiramatsu, Phys. Rev. A **36**, 5349 (1987).
- [11] J. X. Zhong and R. Mosseri, J. Phys.: Condens. Matter **7**, 8383 (1995).
- [12] P. Ribeiro, P. Milman, and R. Mosseri, Phys. Rev. Lett. **93**, 190503 (2004).
- [13] D. R. Hofstadter, Phys. Rev. B **14**, 2239 (1976).
- [14] Y. Aharonov, L. Davidovich, and N. Zagury, Phys. Rev. A **48**, 1687 (1993).
- [15] S. Ryu, A. P. Schnyder, A. Furusaki, and A. W. W. Ludwig, New J. Phys. **12**, 065010 (2010).
- [16] F. Cardano, A. D'Errico, A. Dauphin, M. Maffei, B. Piccirillo, C. de Lisio, G. Salerno, M. Lewenstein, P. Massignan, and E. Santamato, Nat. Commun. **8**, 15516 (2017).
- [17] M. Maffei, A. Dauphin, F. Cardano, et al., New J. Phys. **20**, 013023 (2018).
- [18] See Supplemental Material at [URL will be inserted by publisher] for extended phase diagrams, a movie showing their time evolution, and spectral data.
- [19] P. W. Anderson, Phys. Rev. **109**, 1492 (1958).

## Supplemental Material for “Robust Floquet Topological Phases and Anomalous $\pi$ -Modes in Quasiperiodic Quantum Walks”

### EXTENDED PHASE DIAGRAM

Figure S1 presents the extended phase diagram calculated under periodic boundary conditions with a long-time average ( $T = 2450$  steps) for a system size of  $N = F_{15} = 610$ . Under these conditions, the evolution time exceeds the ballistic transit time, causing the wave packet to wrap around the boundaries and interfere with itself. Consequently, within the metallic phase, these interference effects render the underlying multifractal nature of the spectrum explicitly visible. This visual complexity directly corroborates the fractal nature of the quasiperiodic modulation imprinted on the bulk dynamics. In sharp contrast, the topological phase characterized by the winding number  $\nu = -1$  (yellow regions) remains featureless and robust, exhibiting a mean chiral displacement (MCD) that remains strictly quantized even under such long-time evolution. Interestingly, the intricate boundaries of these topological regions form a fractal pattern reminiscent of Hofstadter’s butterfly, a resemblance that becomes strikingly apparent when the diagram is rotated by  $45^\circ$ . An animation illustrating the development of this phase diagram with increasing averaging time (from  $T = 10$  to 3000) is available as Supplemental Material.

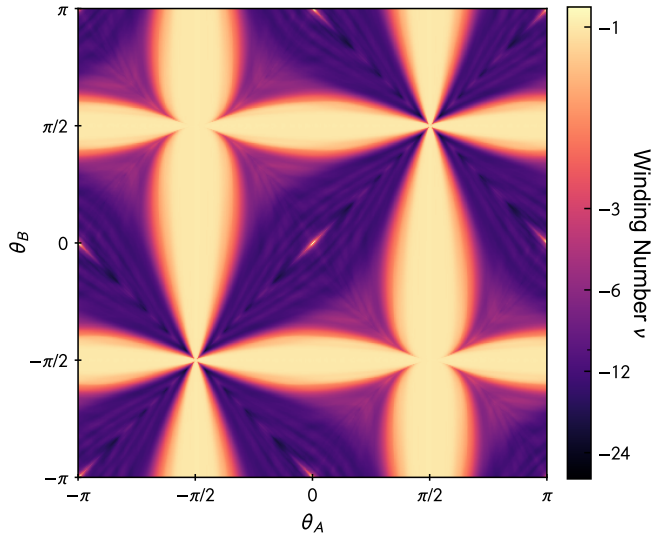


FIG. S1. (Color online) Extended dynamical phase diagram utilizing the mean chiral displacement (MCD) under periodic boundary conditions. The data were computed for a system size of  $N = F_{15} = 610$  with a long-time average over  $T = 2450$  steps. The topological phase (bright yellow region,  $\nu \approx -1$ ) remains strictly quantized and featureless, demonstrating its robustness. In contrast, the metallic and critical phases exhibit intricate self-similar patterns reminiscent of the Hofstadter butterfly. These complex structures arise from the interference of wave packets wrapping around the system boundaries, visually highlighting the fractal nature of the bulk dynamics.

### QUASIENERGY SPECTRUM

Figure S2 presents the quasienergy spectrum as a function of  $\theta_A$ , calculated for a fixed  $\theta_B = 0$ . Two distinct types of isolated modes are clearly resolved within the spectral gaps: zero-energy modes ( $E \approx 0$ ) and  $\pi$ -energy modes ( $E \approx \pm\pi$ ). Both modes exhibit clear exponential spatial localization, identifying them as topological edge states. The simultaneous presence of these boundary modes at both zero and  $\pi$  quasienergies is a hallmark of the Floquet topological phase realized in this Fibonacci quantum walk. As  $\theta_A$  deviates from the deep topological regime ( $\theta \approx \pm\pi/2$ ) towards the phase boundaries, the bulk energy gaps narrow significantly, leading to an increase in the localization length of the edge states. Notably, the gap structure exhibits a high degree of symmetry; the spectral features around  $E = 0$  are virtually identical to those around  $E = \pm\pi$ . In the metallic regions, the spectrum displays a self-similar fragmentation characteristic of a Cantor set. While this fractal structure is physically intriguing, our

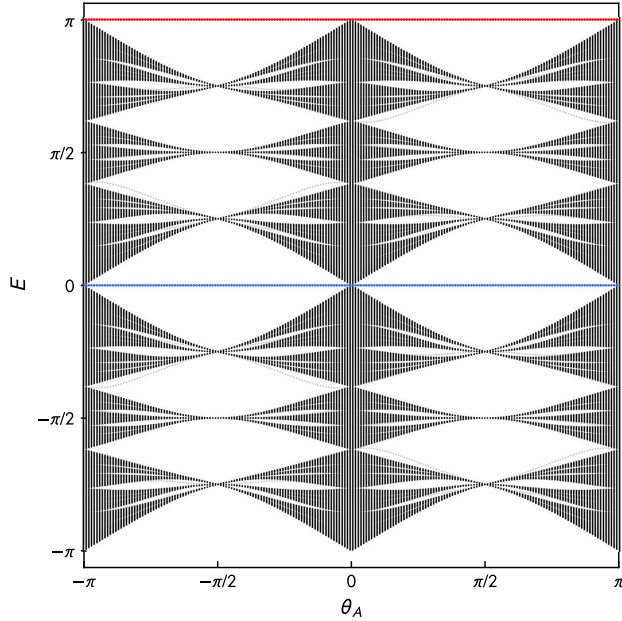


FIG. S2. (Color online) Quasienergy spectrum as a function of  $\theta_A$  for fixed  $\theta_B = 0$ . The bulk bands (black dots) exhibit a fractal structure characteristic of the Fibonacci modulation. Topological edge states are clearly resolved within the gaps centered at  $E = 0$  (blue dots) and  $E = \pi$  (red dots). Note that due to the  $2\pi$ -periodicity of the quasienergy, states at the lower boundary  $E = -\pi$  are mapped to  $E = +\pi$ . As  $\theta_A$  deviates from the deep topological limit ( $\pm\pi/2$ ), the energy gaps narrow, leading to an increase in the localization length of the edge modes.

primary focus in this Letter remains on the robust topological edge states residing within the major energy gaps.